Understanding Protein Lids: Kinetic Analysis of Active Hinge Mutants in Triosephosphate Isomerase†

Jeonghoon Sun and Nicole S. Sampson*

Department of Chemistry, State University of New York, Stony Brook, New York 11794-3400

Received April 14, 1999; Revised Manuscript Received June 18, 1999

ABSTRACT: In previous work we tested what three amino acid sequences could serve as a protein hinge in triosephosphate isomerase [Sun, J., and Sampson, N. S. (1998) *Protein Sci. 7,* 1495−1505]. We generated a genetic library encoding all 8000 possible 3 amino acid combinations at the C-terminal hinge and selected for those combinations of amino acids that formed active mutants. These mutants were classified into six phylogenetic families. Two families resembled wild-type hinges, and four families represented new types of hinges. In this work, the kinetic characteristics and thermal stabilities of mutants representing each of these families were determined in order to understand what properties make an efficient protein hinge, and why all of the families are not observed in nature. From a steady-state kinetic analysis of our mutants, it is clear that the partitioning between protonation of intermediate to form product and intermediate release from the enzyme surface to form methylglyoxal (a decomposition product) is not affected. The two most impaired mutants undergo a change in rate-limiting step from enediol formation to dihydroxyacetone phosphate binding. Thus, it appears that k_{cat}/K_m's are reduced relative to wild type as a result of slower Michaelis complex formation and dissociation, rather than increased loop opening speed.

Proteins are intrinsically flexible molecules. They undergo conformational changes that are frequently an indispensable part of their mechanisms. One important catalytic device that allows a wide range of motion is a hinge. Protein hinges may modulate domain displacements, or conformational changes of protein fragments smaller than domains, i.e., segmental motions (*1*, *2*).

Hinges in small protein segments are frequently found at the ends of Ω loops to form active-site lids. These lids are usually found on the surface of a protein. Their action is critical for subsequent catalysis. Typically, they sequester bound substrates and intermediates from bulk solvent and stabilize catalytic intermediates for efficient catalysis. However, they may also protect hydrophobic active sites from aggregation. A prototypical enzyme with a rigid Ω loop lid that pivots on hinges is triosephosphate isomerase (TIM).[1] This loop, loop 6, is located between β-strand 6 and α-helix 6. This loop is conserved in other α/β TIM barrel proteins. For example, in the α-subunit of tryptophan synthase, loop 6 (residues 177−191), analogous to the active-site loop 6 in TIM, and loop 2 are Ω loops important for catalysis (*3*). Further examples include enolase (*4*), ribulose bisphosphate carboxylase (*5*), and *Yersinia* protein tyrosine phosphatase (*6*−*8*). In these enzymes, Ω loops move 7−10 Å, and recruit electropositive groups to the active site as well as prevent decomposition of reactive intermediates, and stabilize the transition states. Thus, Ω loops are employed to help catalyze a variety of chemical reactions.

Loop 6, the active-site lid of TIM, is composed of 11 amino acids, and opens and closes as a rigid lid (Figure 1). There is a 3 amino acid N-terminal hinge (residues 166−168), a 5 amino acid hydrophobic lid (169−173), and a 3 amino acid C-terminal hinge (174−176). The hydrophobic rigid region that stabilizes bound substrate and intermediate pivots about the two hinges (*9*, *10*). Across evolution, the sequence of the hydrophobic rigid lid is strictly conserved, as is the N-terminal hinge. The C-terminal hinge is conserved, although there is variation. The N-terminal hinge is adjacent to the active-site base, glutamate-165, and this may be the reason for its invariance. The same lid open and closed conformations have been observed in many species by X-ray crystallography, e.g., in chicken, yeast, trypanosome, plasmodium, human, *E. coli*, and *B. stearothermophilus* (*11*−*19*).

In addition to the crystallographic evidence, kinetic, dynamic, and computational experiments have been con-

† This work was supported by a grant from the American Chemical Society−Petroleum Research Fund (N.S.S.) and by a Grant-In-Aid of Research from Sigma Xi (J.S.). The Center for Analysis and Synthesis of Macromolecules (CASM) at Stony Brook is supported by NIH Grant RR02427, and the Center for Biotechnology. NMR spectrometers, centrifuges, and a fluorimeter were purchased with support from the NSF (CHE9413510, CHE9808439, and CHE 9709164).

* To whom correspondence should be addressed. Telephone: (516) 632-7952. Fax: (516) 632-5731. E-mail: nicole.sampson@sunysb.edu.

[1] Abbreviations: TIM, triosephosphate isomerase; WT, wild type; DHAP, dihydroxyacetone phosphate; GAP, (*R*)-glyceraldehyde-3-phosphate; PGH, phosphoglycolohydroxamate; 2-PGA, 2-phospho-D-glycerate; NADH, nicotinamide adenine dinucleotide, reduced form; NAD^+, nicotinamide adenine dinucleotide, oxidized form; GOPDH, α-glycerol-3-phosphate dehydrogenase; GAPDH, glyceraldehyde-3-phosphate dehydrogenase; BHAP, bromohydroxyacetone phosphate; DTT, dithiothreitol; MG, methylglyoxal; P_i, inorganic phosphate; LB, Luria broth; Tris, tris(hydroxymethyl)aminomethane; SDS−PAGE, sodium dodecyl sulfate−polyacrylamide gel electrophoresis; DEAE, diethylaminoethyl; TEA, triethanolamine; EDTA, ethylenediaminetetraacetate; FPLC, fast protein liquid chromatography; NMR, nuclear magnetic resonance.

10.1021/bi990862g CCC: $18.00
Published on Web 08/12/1999

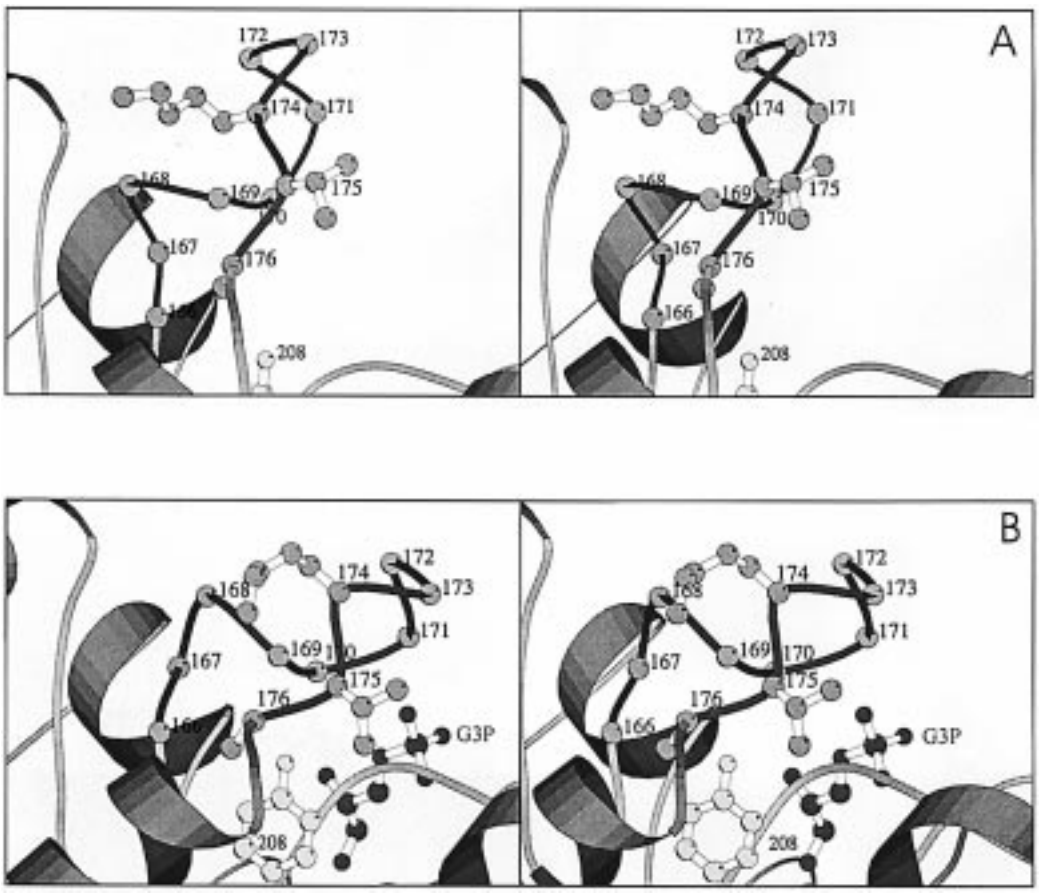

FIGURE 1: Stereo ribbon diagram of TIM with (A) the loop open and (B) the loop closed and glycerol 3-phosphate (G3P) bound in the active site. The open loop is from the same crystal structure determination as the closed. Each subunit of the dimer crystallized in a different loop form. This figure was created with Molscript (*49*) using the coordinates of 6tim.pdb (*13*).

ducted to address the mechanism of the loop in the reaction catalyzed by TIM (*9*, *10*, *20*−*23*). Sampson and Knowles suggested that the loop closes after the Michaelis complex is formed and that loop closure is linked to deprotonation of substrate (*22*). Solid-state NMR experiments by Williams and McDermott elegantly demonstrated that lid motion is not dependent upon the presence of substrate (*23*). The rate of lid movement is on the same time scale as catalysis. Therefore, it is likely that the lid motion is not ligand-gated, but occurs slowly enough for the chemical steps to be completed prior to the lid opening.

Protein hinges are defined by measuring main-chain torsional angle changes between different conformations. Inspection of the hinge amino acid sequences in hinged proteins does not reveal any canonical hinge sequences. Thus, it is not clear what structural and dynamic principles select for the amino acids in a hinge, although the sequences are often strongly conserved throughout the evolution of a specific protein. This is the case for TIM. In previous work, therefore, we tested what three amino acid sequences could serve as a protein hinge in TIM (*24*). We generated a genetic library encoding all 8000 possible 3 amino acid combinations at the C-terminal hinge. Using in vivo complementation with a TIM-deficient strain of *E. coli*, we selected for those combinations of amino acids that formed active mutants. These mutants were classified phylogenetically into six families. Two families resemble wild-type hinges (families 1 and 2, Table 1). Three families (families 3−5, Table 1) represent new types of hinges. Two of these families have aliphatic groups in the third position. The fifth family contains a proline in the middle position, perhaps stabilizing the closed form of the lid. The sixth family is comprised of the only two mutants selected containing glycine. Here we present the kinetic characterization and thermal stabilities of mutants representing each of these families, to understand what properties make an efficient protein hinge.

Table 1: C-Terminal Hinge Mutant Families and the Representative Family Members Studied

family	consensus[a]	hinge sequence of members studied in this work
1	XSS, XSA, XAS	NSS
2	X(β/ϕ)(A/S)	KTA (wild type), RTA, LWA
3	X(A/S)(β/ϕ)	YSL, NSM
4	X(β/ϕ)(L/K/M)	KTK
5	XP(S/N)	NPN
6	1 glycine	EGA

[a] As described in Sun and Sampson (*24*).

EXPERIMENTAL PROCEDURES

Materials. Unless specifically mentioned, all commercial chemicals were used as obtained without further purification. All organic solvents were dried and distilled by standard methods prior to use. Cationic exchange resin Dowex (50WX4-200R, 4% cross-linked), anionic exchange resin Dowex (1X8-400, 8% cross-linked), NADH, NAD^+, DL-glyceraldehyde 3-phosphate (diethyl acetal, monobarium salt), dihydroxyacetone phosphate, 2-phosphoglycolate, so-

dium arsenate, and EDTA were purchased from Sigma Chemical Co. (St. Louis, MO). D_2O was obtained from Cambridge Isotope Laboratories, Inc. (Andover, MA). PGH was a generous gift from Tessa Walters, who synthesized it according to the method of Collins (*48*). BHAP was prepared as described by de la Mare et al. (*25*). α-Glycerol-3-phosphate dehydrogenase (GOPDH) and glyceraldehyde-3-phosphate dehydrogenase (GAPDH) were obtained from Boehringer-Mannheim (Indianapolis, IN), and residual TIM activity was removed by treatment with BHAP for 1 h, followed by ultrafiltration into buffer A for GOPDH and into buffer B for GAPDH. Restriction endonucleases, Klenow fragment, and *T4* DNA ligase were from New England Biolabs (Beverly, MA). Alkaline phosphatase was purchased from United States Biochemical (Cleveland, OH).

The components of reaction buffers used are as follows: buffer A: 100 mM triethanolamine hydrochloride, 10 mM EDTA, pH 7.8 (at 30 °C); buffer B: 100 mM triethanolamine hydrochloride, 1 mM EDTA, pH 7.8, 1 mM DTT (at 30 °C); buffer C: 10 mM Tris-HCl, pH 7.5 (at 25 °C); buffer D: 10 mM Tris-HCl, pH 7.0; buffer E: 10 mM Tris-HCl, 1 mM EDTA, pH 7.6 (at 25 °C). Rich medium was Luria broth (LB) (10 g of tryptone, 5 g of yeast extract, 5 g of NaCl per liter, pH 7). Minimal medium was M63 salts containing CAS amino acids (0.5%, w/v), glycerol (0.2%, w/v), $FeSO_4$ (0.5 mg/L), thiamine (1 mg/L), L-histidine (80 mg/L), streptomycin (100 mg/L), and ampicillin (200 mg/L).

E. coli strain XL1Blue (tet^R) was used for plasmid construction. *E. coli* strain DF502 ($strep^R$, tpi^-, and his^-) was used for in vivo selection, and DF502 was a generous gift from Drs. D. Fraenkel and J. R. Knowles that has been described previously (*26*). The plasmids pBSX1cTIM (wild type and H95N) (*27*) were generous gifts from Drs. E. Komives and J. R. Knowles. The construction of pTMC has been described previously (*24*).

Construction of TIM Mutant Expression Plasmids. The 1.3 kb *Pst*I to *Eco*RI fragment from each of the mutants selected from the pTMC library was subcloned into the 2.8 kb *Pst*I to *Eco*RI fragment from pBSX1cTIM (H95N). The *Age*I site in the random cassette region was used as a restriction marker to verify the presence of the hinge mutant.

Protein Purification of Mutant TIMs. Cell paste (20 g) of DF502(pBSX1c) (NSS, RTA, LWA, NSM, KTK, NPN, YSL, EGA, and wild type) obtained from LB/amp/strep medium (2 L) grown for 24 h was suspended in buffer C (20 mL), and lysed by two passages through a French press at 11 000 psi and 4 °C. Cell debris was removed by centrifugation at 200000*g* for 70 min. All subsequent purification steps were conducted at 4 °C. The supernatant was loaded onto a column (150 mL) of DEAE-cellulose (DE-52, Whatman) preequilibrated with buffer C. The column was washed with the same buffer (150 mL), and the protein was eluted with a linear gradient (0−150 mM, 450 mL + 450 mL) of KCl in buffer C. Fractions were collected and analyzed by SDS−PAGE. Fractions greater than 95% pure were collected, pooled, and desalted using an Amicon concentrator (10 000 MWCO Amicon, Danvers, MA). The sample was loaded onto a second DE-52 column and eluted with a linear gradient (0−100 mM, 450 mL + 450 mL) of KCl in buffer D, and the above procedures were repeated. If needed, the protein was purified once more on a Mono Q 5/5 column in buffer C and eluted using a KCl gradient (0−120 mM, 50 mL + 50 mL). Fractions containing the mutant isomerase were pooled, concentrated by ultrafiltration, and desalted into buffer C. The amount of total protein in the supernatant was determined by Bradford assay (*28*) using wild-type chicken TIM as a standard.

Thermal Stability. The CD spectra were recorded on an AVIV 62A circular dichroism spectrometer (Lakewood, NJ) with a 0.2-mm path length at 2 °C in the presence and absence of 1 mM 2-PGA. For these experiments, solutions of wild-type TIM and the mutant TIMs were equilibrated against buffer E. Protein samples were diluted with the same buffer to a concentration of 40 μM. A base line spectrum of buffer E (with 1 mM 2-PGA for the closed form) was subtracted from the sample spectrum. Temperature denaturation studies in the presence and absence of 1 mM 2-PGA were carried out by monitoring the ellipticity at 222 nm as a function of increasing temperature from 2 to 90 °C with a scan rate of 25 °C per hour. Cuvettes with a 1-cm path length were used, and the protein concentration was 40 μM. The ellipticity of buffer E (with 1 mM 2-PGA for the closed form) was subtracted from the sample ellipticity

Enzyme Assays. Triosephosphate isomerase activity for wild type and the mutants was measured, following a modified protocol of Plaut and Knowles (*29*). One unit of isomerase activity is that amount of enzyme required to convert 1 μmol of GAP to product in 1 min at 30 °C. With GAP as substrate, the assay mixture was comprised of NADH (0.35 mM), GOPDH (0.017 mg/mL), and GAP (0.016−5.0 mM), in 1 mL of buffer A. TIM (1−1.5 ng/mL) was used to initiate the reaction. With DHAP as substrate, the assay mixture was comprised of NAD^+ (0.35 mM), sodium arsenate (10 mM), GAPDH (0.17 mg/mL), and DHAP (0.016−5.5 mM), in 1 mL of buffer B. TIM (3−6 ng/mL) was used to initiate the reaction. Initial rates (the first 10% of reaction) were measured at each substrate concentration with the appearance or disappearance of NADH at 340 nm. The k_{cat} and K_m for GAP were obtained from nonlinear least-squares analyses of plots of S_o (initial substrate concentration) versus v_i (initial velocity). The K_i's for arsenate were determined with five different concentrations of GAP and five different concentrations of arsenate, and the data fit simultaneosly using GraFit (Erithacus Software, Ltd., Stains, U.K.). The K_i's for arsenate were used to calculate the K_m for DHAP.

Inhibition with Phosphoglycolohydroxamate. The concentration of a solution of PGH was determined by colorimetric assay of the inorganic phosphate released by alkaline phosphatase (*30*). Wild-type or mutant isomerases were assayed at three different concentrations of GAP in the presence of five different PGH concentrations. The K_i's were determined by simultaneously fitting the data using GraFit.

Primary Isotope Effect. [1(*R*)-^{2}H]-DHAP was prepared using a modified procedure of Leadlay et al. (*31*). DHAP (80 mg) was equilibrated in 3 mL of D_2O with 50 μg of wild-type rabbit TIM under argon in a 10kD centricon (Amicon, Danvers, MA) and incubated at 37 °C for 2 h. After removing TIM by ultrafiltration, BHAP-treated aldolase (50 μg) was added to the DHAP and incubated at 37 °C for 2 h. The aldolase was removed by ultrafiltration. The mixture of [1(*R*)-^{2}H]-DHAP and fructose 1,6-bisphosphate was dissolved in 100 mL of water and loaded onto a 6 cm × 10 cm anion exchange column (AG-1-X8 Cl^- preequilibrated

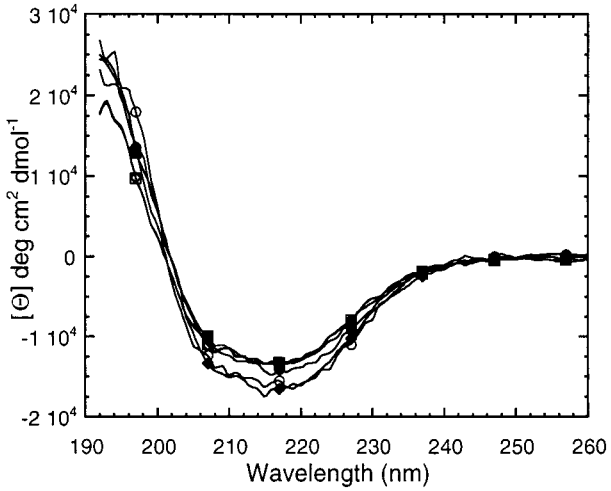

FIGURE 2: CD spectra of wild-type and mutant open forms. (●) Wild type; (○), NSS; (■) YSL; (□) KTK; (◇) NPN; (◆) EGA.

in pH 3.8 HCl), washed with 20 mL of pH 3.2 HCl, and eluted with 60 mL of pH 1.7 HCl. The absorbance of the eluate was monitored at 220 nm. The DHAP-containing fractions were collected, neutralized with 2 N NaOH, and concentrated by lyophilization. The ^{1}H NMR spectrum showed 95% incorporation of D. Using the synthesized [1(*R*)-^{2}H]-DHAP as a substrate, initial rates were measured as described above. The primary isotope effect was calculated with GraFit using two parameters: fraction of isotope, f_i, and substrate concentration, S_o, and fitting to the combined initial velocity v_i data sets for [^{2}H]-DHAP and [^{1}H]-DHAP.

Methyl Glyoxal Formation. Methyl glyoxal formation was monitored at a single substrate concentration using the method of Richard (*32*). The enzyme concentration was 30 μM, and the [^{32}P]-DHAP concentration was 0.15 nM. Time points were collected over 20 h.

Detection of Substrate Exchange. [1(*R*)-^{1}H]-DHAP (5 mM) was dissolved in D_2O at pH 7.5 (uncorrected). TIM (wild type or mutant) was added (0.4 μg/mL). The ^{1}H NMR spectrum was acquired at 300 MHz as a function of time. Between acquisitions, the sample was incubated at 30 °C. The integrated intensity of the (1*R*)-^{1}H resonance at 3.44 ppm was plotted as a function of time, and the rates of wild-type catalyzed exchanged were compared to the mutant rates.

RESULTS

Protein Expression and Purification. TIM hinge mutants that had been previously selected as active (*24*) were subcloned into pBSX1cTIM. All of the hinge mutants were expressed at 80−120 mg/L culture after 20−24 h and were purified to homogeneity. The anion exchange elution profiles of the mutants correlated to their expected change in p*I* relative to wild type. The secondary structure of the mutants was determined using circular dichroism. Spectra were acquired from 190 to 260 nm at 2 °C (Figure 2). All of the mutants appeared to be folded identically to wild type.

Steady-State Kinetics. The steady-state rate constants for the wild-type isomerase and the representative active hinge mutants were determined in both the forward (DHAP → GAP) and the reverse (GAP → DHAP) directions. These results are summarized in Figures 3 and 4. In addition, the affinity (K_i) for the intermediate analogue, PGH, was

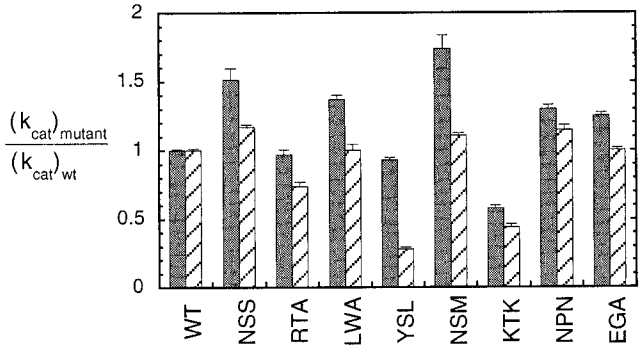

FIGURE 3: Bar graph representation of k_{cat} for the mutants relative to wild type. Solid: GAP as substrate, $(k_{cat})_{wt} = 4000 \pm 40$ s^{-1}; striped: DHAP as substrate, $(k_{cat})_{wt} = 540 \pm 7$ s^{-1}.

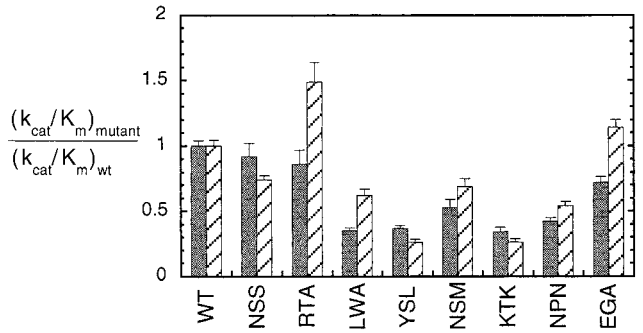

FIGURE 4: Bar graph representation of k_{cat}/K_m for the mutants relative to wild type. Solid: GAP as substrate, $(k_{cat}/K_m)_{wt} = (7.9 \pm 0.3) \times 10^6$ M^{-1} s^{-1}; striped: DHAP as substrate, $(k_{cat}/K_m)_{wt} = (2.3 \pm 0.1) \times 10^5$ M^{-1} s^{-1}.

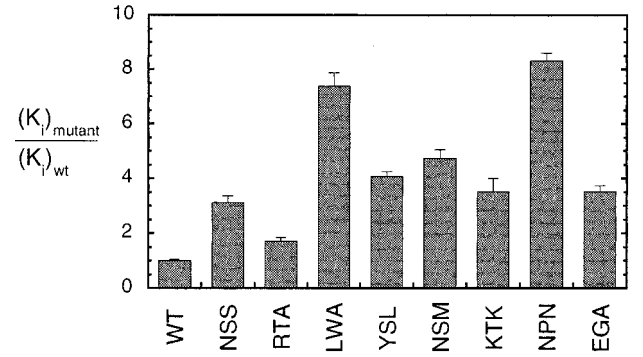

FIGURE 5: Bar graph representation of K_i for PGH for the mutants relative to wild type, $(K_i)_{wt} = 8.5 \pm 0.1$ μM.

measured using GAP as a substrate, and these data are summarized in Figure 5. Methylglyoxal and P_i are the byproducts that result from decomposition of the enediol intermediate. The rate of P_i elimination by the mutants is the same as that measured for wild type, 1.7 M^{-1} s^{-1}. That is, the amount of methylglyoxal produced by wild type and the mutants is less than 1 methylglyoxal in 10^5 turnovers.

Primary Kinetic Isotope Effect. We examined whether the hinge mutations altered the rate-determining step of the catalyzed reactions. The primary kinetic isotope effect was measured using [(1*R*)-^{2}H]-DHAP as the substrate (Table 2). NSS, NPN, LWA, RTA, and NSM showed significant primary isotope effects that were similar to wild type, whereas YSL and KTK showed no primary deuterium kinetic isotope effects. There was a primary kinetic isotope effect for EGA; however, the magnitude was reduced compared to wild type. In the wild-type reaction, the (1*R*)-^{2}H is rapidly exchanged with solvent and does not appear in the product

Table 2: Isotope Effects on Wild Type and Hinge Mutants

family	mutants	$^{D}(V/K)^{a}$
1	NSS	3.91 ± 0.03
2	KTA (WT)	3.56 ± 0.10
2	RTA	2.92 ± 0.05
2	LWA	3.41 ± 0.07
3	YSL	1.08 ± 0.03
3	NSM	2.70 ± 0.40
4	KTK	1.12 ± 0.01
5	NPN	2.97 ± 0.06
6	EGA	1.43 ± 0.01

[a] Assayed using [1(*R*)-^{2}H]-DHAP; $^{D}(V)$ is the same as $^{D}(V/K)$.

Table 3: T_m of Representative Hinge Mutants

family	mutants	open[a]	closed[b]
1	NSS	58.3 ± 0.1	69.0 ± 0.1
2	KTA (WT)	58.4 ± 0.1	73.6 ± 0.1
3	YSL	56.1 ± 0.1	67.2 ± 0.1
4	KTK	56.0 ± 0.1	67.9 ± 0.1
5	NPN	57.3 ± 0.1	65.7 ± 0.1
6	EGA	58.8 ± 0.1	71.6 ± 0.1

[a] Measured from 2 to 90 °C at pH 7.6. [b] As in (*a*); measured in the presence of 1 mM 2-PGA.

(*31*). Using ^{1}H NMR spectroscopy, we measured the rate of substrate (1*R*)-^{1}H exchange with $^{2}H_2O$ and determined that all of the mutants exchange with solvent at the same rate as wild type, $t_{1/2} = 0.5$ h.

Thermal Stability. Thermal denaturation studies were carried out in the temperature range of 2−90 °C and monitored at 222 nm. In addition to wild type, NSS, NPN, YSL, and KTK were studied. These mutants were chosen as single representatives of each family. The melting temperatures in both the absence and presence of 2-PGA (1 mM) were determined at a single protein concentration (1.6 μM) (Table 3). This concentration is 10^5 orders of magnitude higher than the estimated K_d (10 pM) for the dimer−monomer equilibrium (*33*). Consequently, the measured T_m's were not expected to be dependent on the protein concentration in the range studied. As shown in Figure 6, there were no significant changes in the cooperativity of the melting curves for each of the mutants investigated. All of the mutants and wild type were irreversibly denatured at 90 °C.

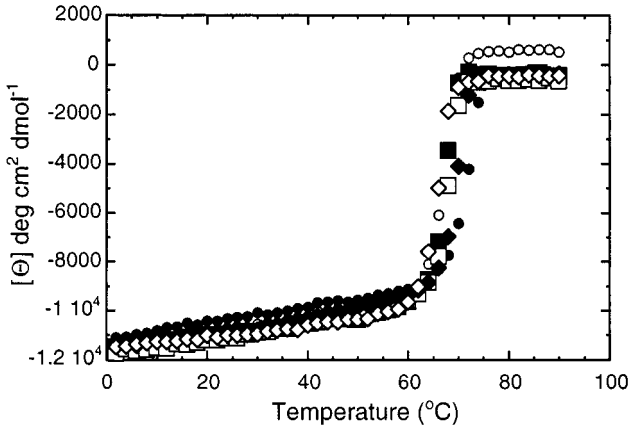

FIGURE 6: Melting curves of mutant and wild-type closed forms (measured in the presence of 1 mM 2-PGA). (●) Wild type; (○) NSS; (■) YSL; (□) KTK; (◇) NPN; (◆) EGA.

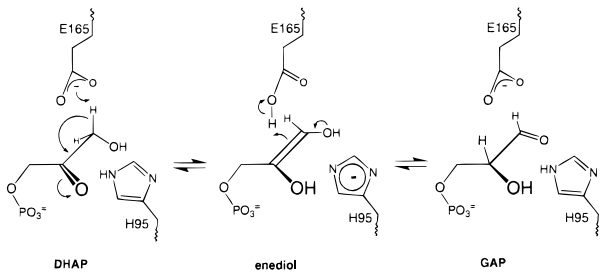

FIGURE 7: Reaction catalyzed by TIM.

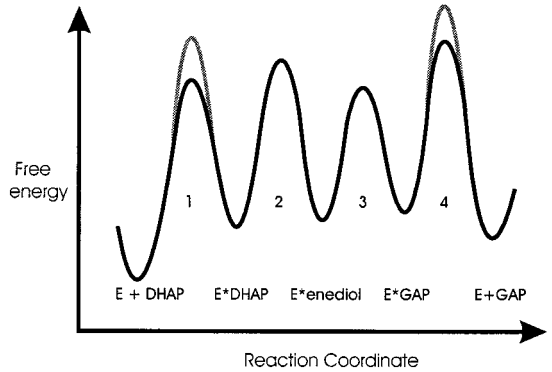

FIGURE 8: Free energy profile for wild-type chicken isomerase adapted from Albery and Knowles (*36*). The standard state is 40 μM triosephosphates (*50*). The gray lines denote the barriers that have been raised by hinge mutation.

DISCUSSION

TIM is a dimeric glycolytic enzyme that catalyzes the interconversion of dihydroxyacetone phosphate (DHAP) and (*R*)-glyceraldehyde-3-phosphate (GAP) via an enediol(ate) intermediate with extremely high efficiency (Figure 7) (*34*, *35*). The free energy profile of the catalytic process has been determined (Figure 8) (*36*), and the extensive kinetic characterization of this enzyme has revealed that the enzyme has evolved to an optimized form (*37*, *38*). The criteria for optimization are 2-fold: that the rate is limited by the diffusion of the less stable substrate on and off of the enzyme, and that no intermediate accumulates on the enzyme. Its representative canonical barrel, $(\beta\alpha)_8$, is observed in more than 20 different classes of enzyme (*39*, *40*). The functionally important loop, loop 6, connects β-strand 6 and α-helix 6 and covers the active site. This loop is mobile, and has primarily been observed in two conformations: the open (Figure 1A) and, upon movement of the tip of the loop about 7 Å, the closed (Figure 1B). In the closed form, the loop clamps down over the active site, effectively blocking access of solvent to the active site. A loop half-closed intermediate form has also been crystallized (*13*). In all three structures, the conformation of the loop remains the same; only the dihedral angles about the hinges change.

The first kinetic step in catalysis by triosephosphate isomerase is binding of substrate to the enzyme; the rate of this step is at the limit of bimolecular diffusion. The second step is deprotonation and enolization of the substrate to form the enediol intermediate (*36*). This chemistry is effected by the movement of glutamate-165 2 Å toward the substrate into a position for facile deprotonation of substrate (*25*, *41*, *42*) and by the orientation of histidine-95 to polarize the substrate carbonyl (*43*−*46*). Once formed, the enediol intermediate is sequestered on the enzyme surface and protected from water by the 11 amino acid loop (*20*). In

solution, the intermediate decomposes at 100 times the rate it is reprotonated. The function of the loop, as deduced from X-ray crystallography, was confirmed by kinetic experiments with a loop-deleted mutant enzyme. Removal of the loop results in an impaired enzyme that can no longer enolize the substrate to form intermediate effectively, or reprotonate the intermediate to form product. Consequently, the enediol decomposes into methylglyoxal and inorganic phosphate (*20*). These species are the same decomposition products observed when the enediol is formed in solution (*32*). There are, at minimum, two functions of the loop: (1) to constrain the intermediate in a conformation unfavorable for elimination on the surface of the enzyme; and (2) to sequester the intermediate from solvent, thus lowering the energy required for enolization.

Further mutagenesis experiments with the loop revealed that only those hydrogen-bonding interactions between the closed loop and the protein appear critical for catalysis (*21*). Removal of one hydrogen bond, between the hydroxyl of tyrosine-208 and the amide nitrogen of alanine-176, a constituent of the loop (Figure 1), had a dramatic effect on catalysis; the reaction rate was lowered 2000-fold. Thorough kinetic investigation of this Y208F mutant revealed that the binding (substrate association) step was not affected by the mutation, but that the energy required for enolization was approximately 4.6 kcal greater than in the wild-type enzyme. Measurement of the effects of added viscosogens (glycerol or sucrose) on the reaction revealed that the rate-limiting enolization step is viscosity dependent (*22*). Because the transition states for enolization were clearly rate-limiting for the mutant Y208F enzyme, it was concluded that the addition of viscosogen slowed the movement of the loop during enolization of the substrate. It is not known whether the wild-type loop closes during substrate binding or during enolization. Furthermore, solid-state NMR experiments have been used to demonstrate that loop motion is on the time scale of catalytic turnover but is not ligand-gated (*23*). Hence, loop closure is not triggered by binding of substrate or product. Rather, the loop is constantly opening and closing, and enolization only occurs when the lid is closed.

A critical element for effective enzyme function is that the loops open and close with the appropriate rate constant. Previously, we undertook a study to determine how many three amino acid combinations could function as a hinge for loop 6 in triosephosphate isomerase. Inspection of more than 60 sequences from diverse species suggested that the number of combinations would be limited. However, in vivo complementation of an 8000 member library (all 3 amino acid combinations) revealed that there was a greater number of functioning hinges than predicted. Interestingly, glycine-rich hinge mutants were not observed. That is, the amino acid that allows the greatest degree of conformational flexibility does not make the most effective hinge. This observation is consistent with the requirement that the rate of loop movement corresponds to the rate of catalysis. The active hinge mutants were classed into six families (Table 1). In this work, we have kinetically characterized representative members of each family in order to determine if there are subtle differences between those mutants observed in nature and those that are not.

In the GAP to DHAP direction, some mutants (NSS, LWA, NSM, NPN, and EGA) had higher k_{cat}'s than wild type. For wild type, the rate-determining step at high GAP (substrate) concentration is protonation of the enediol intermediate to form DHAP (Figure 8) (*37*). Thus, these hinge mutations slightly improve the rate of a chemical step in the catalyzed reaction. However, except for NSS which is the same as wild type, these mutants are slightly less active than wild type at low GAP concentrations, i.e., k_{cat}/K_m. It appears that substrate specificity is sacrificed in order to obtain modest improvements in chemical efficiency. In the DHAP to GAP direction, none of the mutants have a k_{cat} or k_{cat}/K_m larger than wild type, except RTA which is classed in family 2, 'wild type'. Five of the mutants, LWA, YSL, NSM, KTK, and NPN, actually have reduced k_{cat}/K_m's. If these rate reductions were a result of faster loop opening after formation of the intermediate, then we would expect to see an accompanying increase in MG formation. That is, the partitioning between desired product and decomposition product would be altered in favor of the decomposition product. The rates of MG formation for the hinge mutants are identical to wild type. Thus, it appears that the rate of loop opening has not been increased in these hinge mutants.

We investigated the effect of the hinge mutations on enolization using deuterated DHAP. Because the labile deuteron (1*R*-^{2}H) is lost to solvent upon formation of the enediol intermediate, the unusual situation arises that the kinetic isotope effect is only a reflection on the energetics of the first two catalytic steps (*31*). If we consider the case in which step 4 (Figure 8) is overall rate-limiting, a kinetic isotope effect on k_{cat}/K_m or k_{cat} will be observed if step 2 is slower than step 1. Even though step 2 (the deuterium-sensitive step) is not rate-limiting overall, it determines the flux of substrate to form enediol. If the substrate is deuterated, the flux is reduced. After formation of the intermediate, the deuterium is lost to solvent, and thus the rate of enediol conversion to GAP is independent of isotopic label on the substrate. The overall rate is determined by the product of the flux into the intermediate enediol and the rate of enediol conversion to free GAP. In contrast, if step 1 is slower than step 2, a kinetic isotope effect on k_{cat}/K_m or k_{cat} will not be observed. The enediol and bound DHAP are essentially in equilibrium with one another and the solvent, and the rate of DHAP deprotonation (step 2) does not affect the flux into the intermediate, nor the overall rate (k_{cat}/K_m or k_{cat}) (*38*).

The deuterium kinetic isotope effects (Table 2) indicate that for wild type and all of the mutants, except YSL and KTK, deprotonation of DHAP is slower than formation of the DHAP Michaelis complex. For these two mutants, it appears that formation of the Michaelis complex is slower, because a kinetic isotope effect is no longer observed on k_{cat}/K_m or k_{cat}. These two mutations also result in the largest decreases in k_{cat}/K_m. Other mutants also show a decrease in k_{cat}/K_m; however, DHAP deuterium kinetic isotope effects are observed. This suggests the decreases in k_{cat}/K_m are primarily due to the rate of GAP release from the product Michaelis complex being reduced. Taken together with the MG partitioning experiments, it appears that the hinge mutations reduce the rate of substrate binding and product release, rather than increase the rate of loop opening (Figure 8, gray lines). The reduced rate of Michaelis complex formation may be a result of slower loop closure or steric hindrance. That is, the number of substrate−enzyme colli-

sions that result in productive binding may be reduced as a result of hinge mutation.

Although NMR spectroscopic evidence suggests that the open and closed conformations both exist in the absence of substrate or inhibitors, the open conformation is the predominant species (*23*). That is, in the absence of substrate, the open conformation is thermodynamically more stable. This is consistent with the observation of the open form in unliganded protein X-ray crystal structures. Conversely, in the presence of enzyme intermediate or intermediate analogue, the closed form is stabilized, and predominates. 2-PGA is one such inhibitor that stabilizes the closed conformation (*47*); PGH is another (*48*). Thus, the T_m's measured in the absence of 2-PGA represent the T_m's of the open conformation. These T_m's did not change significantly upon mutation of the C-terminal hinge. In contrast, the T_m's of the closed conformation stabilized by 2-PGA were 5−8 °C lower than wild type (Table 3). The decrease in closed form stability measured by thermal melting parallels the decrease in affinity (K_i) for PGH measured kinetically. There is no correlation, however, between the thermal stability of the closed form and kinetic activity, i.e., k_{cat} or k_{cat}/K_m. That is, small decreases in enzyme-bound intermediate stability as estimated from inhibitor binding do not affect the rates at which deprotonation/reprotonation of substrate/product or substrate/product diffusion occur. Moreover, the partitioning between desired product and decomposition product is not altered by decreased stability of the bound intermediate. These results further support the suggestion that the hinge mutants do not affect the free energy of the transition states for chemical catalysis.

Our experiments suggest that there are many hinge sequences that open at a rate amenable to efficient catalysis. It may be that the rate of loop movement is controlled more by protein−loop interactions than the hinge itself (*21*, *22*). There appear to be, nevertheless, other criteria for selection of an optimal protein hinge. From a kinetic analysis of our mutants, it is clear that the partitioning between protonation of intermediate and intermediate release to form MG is not affected. The two most impaired mutants have undergone a change in rate-limiting step from enediol formation to DHAP binding. Thus, it appears that the hinge−mutant k_{cat}/K_m's are reduced as a result of slower Michaelis complex formation and dissociation, not increased loop opening speed. The absence of hinge families 3−6 in nature may be due to evolutionary selection for the maximal rate of formation of the Michaelis complex. The slower Michaelis complex formation may be a result of slower loop closure or due to steric interference upon substrate−enzyme collision. Analysis of these mutants by crystallographic structure determination and direct measurement of loop movement rates will further elucidate the sequence criteria for a protein hinge. This analysis is in progress.

ACKNOWLEDGMENT

We thank Prof. Daniel Raleigh for helpful discussions, and the use of his CD spectrophotometer.

SUPPORTING INFORMATION AVAILABLE

A table of the steady-state rate and inhibition constants for all of the mutants is available. This material is available free of charge via the Internet at http://pubs.acs.org.

REFERENCES

1. Gerstein, M., Lesk, A. M., and Chothia, C. (1994) *Biochemistry 33*, 6739−6749.
2. Gerstein, M., and Krebs, W. (1998) *Nucleic Acids Res. 26*, 4280−4290.
3. Rhee, S., Parris, K. D., Hyde, C. C., Ahmed, S. A., Miles, E. W., and Davies, D. R. (1997) *Biochemistry 36*, 7664−7680.
4. Reed, G. H., Poyner, R. R., Larsen, T. M., Wedekind, J. E., and Rayment, I. (1996) *Curr. Opin. Struct. Biol. 6*, 736−743.
5. Larson, E. M., Larimer, F. W., and Hartman, F. C. (1995) *Biochemistry 34*, 4531−4537.
6. Jia, Z., Barford, D., Flint, A. J., and Tonks, N. K. (1995) *Science (Washington, D.C.) 268*, 1754−1758.
7. Keng, Y. F., Wu, L., and Zhang, Z. Y. (1999) *Eur. J. Biochem. 259*, 809−814.
8. Wang, F., Li, W. Q., Emmett, M. R., Hendrickson, C. L., Marshall, A. G., Zhang, Y. L., Wu, L., and Zhang, Z. Y. (1998) *Biochemistry 37*, 15289−15299.
9. Joseph, D., Petsko, G. A., and Karplus, M. (1990) *Science (Washington, D.C.) 249*, 1425−1428.
10. Derreumaux, P., and Schlick, T. (1998) *Biophys. J. 74*, 72.
11. Delboni, L. F., Mande, S. C., Rentier-Delrue, F., Mainfroid, V., Turley, S., Vellieux, F. M., Martial, J. A., and Hol, W. G. J. (1995) *Protein Sci. 4*, 2594−2604.
12. Mande, S. C., Mainfroid, V., Kalk, K. H., Goraj, K., Martial, J. A., and Hol, W. G. (1994) *Protein Sci. 3*, 810−821.
13. Noble, M. E. M., Wierenga, R. K., Lambeir, A.-M., Opperdoes, R. R., Thunnissen, A.-M. W. H., Kalk, K. H., Groendijk, H., and Hol, W. G. J. (1991) *Proteins: Struct., Funct., Genet. 10*, 50−69.
14. Noble, M. E. M., Zeelen, J. P., and Wierenga, R. K. (1993) *Proteins: Struct., Funct., Genet. 16*, 311−326.
15. Wierenga, R. K., Noble, M. E. M., Vriend, G., Nauche, S., and Hol, W. G. J. (1991) *J. Mol. Biol. 220*, 995−1015.
16. Lolis, E., and Petsko, G. A. (1990) *Biochemistry 29*, 6619−6625.
17. Lolis, E., Alber, T., Davenport, R. C., Rose, D., Hartman, F. C., and Petsko, G. A. (1990) *Biochemistry 29*, 6609−6618.
18. Velanker, S. S., Ray, S. S., Gokhale, R. S., Suma, S., Balaram, H., Balaram, P., and Murthy, M. R. (1997) *Structure 5*, 751−761.
19. Zhang, Z., Sugio, S., Komives, E. A., Liu, K. D., Knowles, J. R., Petsko, G. A., and Ringe, D. (1994) *Biochemistry 33*, 2830−2837.
20. Pompliano, D. L., Peyman, A., and Knowles, J. R. (1990) *Biochemistry 29*, 3186−3194.
21. Sampson, N. S., and Knowles, J. R. (1992) *Biochemistry 31*, 8482−8487.
22. Sampson, N. S., and Knowles, J. R. (1992) *Biochemistry 31*, 8488−8494.
23. Williams, J. C., and McDermott, A. E. (1995) *Biochemistry 34*, 8309−8319.
24. Sun, J., and Sampson, N. S. (1998) *Protein Sci. 7*, 1495−1505.
25. de la Mare, C., Coulson, A. F. W., Knowles, J. R., Priddle, J. D., and Offord, R. E. (1972) *Biochem. J. 129*, 321−331.
26. Straus, D., and Gilbert, W. (1985) *Proc. Natl. Acad. Sci. U.S.A. 82*, 2014.
27. Hermes, J. D., Parekh, S. M., Blacklow, S. C., Köster, H., and Knowles, J. R. (1989) *Gene 84*, 143.
28. Bradford, M. M. (1976) *Anal. Biochem. 72*, 248−254.
29. Plaut, B., and Knowles, J. R. (1972) *Biochem. J. 129*, 311−320.
30. Ames, B. N. (1966) *Methods Enzymol. 8*, 115−118.
31. Leadlay, P. F., Albery, W. J., and Knowles, J. R. (1976) *Biochemistry 15*, 5617−5620.
32. Richard, J. P. (1991) *Biochemistry 30*, 4581−4585.
33. Borchert, T. V., Abagyan, R., Jaenicke, R., and Wierenga, R. K. (1994) *Proc. Natl. Acad. Sci. U.S.A. 91*, 1515−1518.
34. Rose, I. A. (1962) *Brookhaven Symp. Biol. 15*, 293−209.
35. Rieder, S. V., and Rose, I. A. (1959) *J. Biol. Chem. 234*, 1007−1010.
36. Albery, W. J., and Knowles, J. R. (1976) *Biochemistry 15*, 5627−5631.

37. Albery, W. J., and Knowles, J. R. (1976) *Biochemistry 15*, 5631−5640.
38. Knowles, J. R., and Albery, W. J. (1977) *Acc. Chem. Res. 10*, 105−111.
39. Janecek, S., and Bateman, A. (1996) *Biologia 51*, 613−628.
40. Farber, G. K., and Petsko, G. A. (1990) *Trends Biochem. Sci. 15*, 228−234.
41. Waley, S. G., Mill, J. C., Rose, I. A., and O'Connell, E. L. (1970) *Nature (London) 227*, 181.
42. Raines, R. T., Sutton, E. L., Straus, D. R., Gilbert, W., and Knowles, J. R. (1986) *Biochemistry 25*, 7142−7154.
43. Belasco, J. G., and Knowles, J. R. (1980) *Biochemistry 19*, 472−477.
44. Nickbarg, E. B., and Knowles, J. R. (1988) *Biochemistry 27*, 5939−5947.
45. Komives, E. A., Chang, L. C., Lolis, E., Tilton, R. F., Petsko, G. A., and Knowles, J. R. (1991) *Biochemistry 30*, 3011−3019.
46. Lodi, P. J., and Knowles, J. R. (1991) *Biochemistry 30*, 6948−6956.
47. Wolfenden, R. (1969) *Nature 223*, 704−705.
48. Collins, K. D. (1974) *J. Biol. Chem. 249*, 136−142.
49. Kraulis, P. J. (1991) *J. Appl. Crystallogr. 24*, 946−950.
50. Williamson, J. R. (1965) *J. Biol. Chem. 240*, 2308−2321.

BI990862G